J Mater Sci (2012) 47:420–428
DOI 10.1007/s10853-011-5815-y

Polyaniline–sodium montmorillonite clay nanocomposites: effect of clay concentration on thermal, structural, and electrical properties

Samrana Kazim · Shahzada Ahmad · Jiri Pfleger · Josef Plestil · Yogesh M. Joshi

Received: 16 May 2011 / Accepted: 21 July 2011 / Published online: 6 August 2011

Abstract A simple and facile method was used to synthesize polyaniline (PANI) nanocomposites with sodium montmorillonite clay (Na^+-MMT) using in situ intercalative oxidative polymerization. Aniline was admixed with Na^+-MMT at various concentrations, keeping the aniline monomer in the reaction mixture constant. The intercalation of PANI into the clay layers was confirmed by X-ray diffraction studies in conjugation with electron microscope techniques and FTIR spectra, particularly by the narrowing of the Si–O stretching vibration band confirmed the interaction between PANI and the clay. The employed route offers the possibility to improve the thermal properties with simultaneously controlled electrical conductivity. Thermal studies show an improved thermal stability of the nanocomposites relative to the pure PANI. Depending on the loading of the clay, the room temperature conductivity values of these nanocomposites varied between 2.0×10^{-4} and 7.4×10^{-4} S cm^{-1}, with the maximum at 44 wt% PANI concentration. The decrease of electrical conductivity at high PANI concentration was ascribed to the decrease of the structural ordering of PANI in the nanocomposite.

S. Kazim (✉) · J. Pfleger · J. Plestil
Department of Optoelectronic Phenomena and Materials, Institute of Macromolecular Chemistry, ASCR, Heyrovsky Sq. 2, 162 06 Prague 6, Czech Republic
e-mail: kazim.samrana@gmail.com

S. Kazim · Y. M. Joshi
Department of Chemical Engineering, Indian Institute of Technology, Kanpur 208016, India

S. Ahmad
Max Planck Institute for Polymer Research, Ackermannweg 10, 55128 Mainz, Germany

Introduction

Polyaniline (PANI) is an extensively exploited conducting polymer because of its economic viability, easy processability, good stability, and controllable electrical conductivity. Various dopants were employed to tune the conductivity of PANI, its composites and blends to meet technological requirements [1–6]. These properties made possible to use PANI as an electrode in lithium ion batteries [7], dye sensitized solar cells [8], microwave absorber in electromagnetic shielding [9], anticorrosion coatings [10], sensors [11], and electrochromic devices [12]. In order to further improve the properties of PANI, its confinement into nanoscale inorganic environments has been adopted. Hybrid composites such as lamellar nanocomposites based on PANI with various layered host materials, such as oxyhalides (FeOCl) [13], transition metal oxides (V_2O_5, MoO_3) [14, 15], and chalcogenides (MoS_2, $MnPS_3$) [16–18] have been explored. These PANI/inorganic nanocomposites possess a variety of unique characteristics based on interactions at a molecular level. Thus, the combination of a conducting polymer with an inorganic host-layered silicate provides a way for obtaining new conducting nanocomposites with much improved mechanical, thermal, electrical, and optical properties. Among other inorganic layered host materials, montmorillonite (MMT) clay is one of the most abundantly employed one owing to its low cost, good chemical resistance, and its ability to be intercalated efficiently. Nanocomposites composed of MMT clay with various polymers and copolymers, such as polyamide 6/polystyrene blend [19], epoxy resin [20], polyurethane [21], and polyester-based polyurethane [22] have been reported, which demonstrate novel properties, such as improved tensile strength and modulus, flame retardancy, reduced gas permeability, improved adhesive properties,

and decreased thermal expansion coefficient compared with classical composites because of the high aspect ratio of individual platelets and the large available surface area [13–22]. Considering these facts in this study, MMT clay was exploited as an inorganic host for the synthesis of PANI-based nanocomposites. Intercalation polymerization is a promising strategy to confine the polymer chains within the nanometer size inorganic galleries. In the intercalation polymerization, the inorganic layers serve as a template, in which organic guest monomer in sub nanometer size is introduced. The template can provide a synergistic effect that leads to structures with properties that cannot be attained from the individual counterparts, e.g., to a high degree of structural ordering and consequently to a high anisotropy of electrical conductivity [23] and high thermal and oxidative stability [24–27].

Intercalated and/or exfoliated nanocomposites can be prepared by intercalation polymerization depending upon monomer/clay ratio. In the past, PANI/MMT were synthesized by emulsion intercalation [28–31], electrochemical [32, 33], inverse emulsion polymerization [34], in situ intercalation [35, 36], and mechanochemical intercalation method [37, 38]. A higher intercalation level of PANI inside the clay gallery was achieved when the MMT was chemically modified by various organic molecules before the polymerization [39–41].

Lee et al. synthesized intercalated PANI/MMT nanocomposites with various PANI fractions [42] and found that the type of physical interaction between the clay and PANI as well as the electrical conductivity and thermal stability of the composites are consistently related to the structure of the nanocomposites as found from X-ray diffraction analysis. Celik et al. [43] also found that the intercalated PANI/MMT nanocomposites have high thermal stability because of the intercalation of PANI between clay layers, which was confirmed by the increase in interlayer spacing by about 0.53 nm.

Nascimento et al. [44] followed a protocol for the preparation of PANI–MMT composites reported by Kim et al. [28, 29], and using combination of X-ray diffraction, scanning electron microscopy, and X-ray absorption near silicon *K*-edge data, they found that the morphology of PANI–MMT nanocomposites depends strongly on the PANI/MMT content ratio and confirmed that PANI has an emeraldine salt (ES) form for all PANI–MMT materials prepared. The electrical conductivity values of composites increased with increased PANI content from 10^{-4} to 10^{-1} S cm^{-1}, with a typical percolation behavior. The percolation threshold was occured below 60 wt% of the PANI concentration.

Recently, Bober et al. [45] reported the series of PANI/MMT nanocomposites prepared by surface and intercalative polymerization methods using various types of clay with the constant molar ratio of aniline hydrochloride/APS oxidant, 0.2:0.25. The conductivity of nanocomposites in both approaches was found to be lower than pure PANI.

The intercalated PANI/MMT nanocomposites preparation and properties reported till the date either have used different oxidants, or varied the aniline monomer amount with respect to the clay, or monomer to dopant ratio. The conductivity of these nanocomposites showed lower values than pristine PANI [28, 29, 36, 45]. The reason could be the lack of connectivity between intercalated PANI chains [35, 36], or a change in the nature of these polymeric chains.

However, in previous articles, the effect of clay loading has been studied only for PANI/MMT nanocomposites prepared by ex-situ polymerization or emulsion intercalation polymerization, and systematic studies showing the dependence of structure on the clay concentration and the effect of structure variation on the thermal and electrical properties of the composite are rather scarce and show diverse results.

Contrary to the previous studies, the objective in this study is to investigate a possible influence of MMT clay loading on extent of intercalation, morphology, electrical and thermal properties of intercalated PANI/MMT nanocomposites prepared by in-situ intercalative polymerization using APS oxidant. An attempt has been made to understand the relationship between clay loading and the structure–property relationship. Surprisingly, we observed that the conductivity increases with increasing MMT concentration for MMT content up to 60 wt%, showing higher value of the conductivity for the composite than for the pure PANI. The enhanced thermal stability along with the increased conductivity of these nanocomposites might be important for many industrial applications like EMI shielding or polymer electrodes for batteries and solar cells.

Experimental section

Materials

Aniline (Merck, Germany) was distilled twice under reduced pressure before use. Hydrochloric acid (HCl) used as a dopant and ammonium persulfate (APS) ($(NH_4)_2S_2O_8$) as an oxidant (Merck, Germany) were used as received. Commercial sodium montmorillonite (Na^+-MMT), Cloisite® Na^+ Nanoclay, $Na_{0.65}[Al, Fe]_4Si_8O_{20}(OH)_2$ was supplied by the Southern Clay Product, USA, and was grinded and dried in a vacuum oven at 120 °C for 24 h before use.

Synthesis of PANI/MMT clay nanocomposites (PNC)

PANI/MMT nanocomposites were prepared by the initial intercalation of MMT using aniline monomer and subsequent polymerization of aniline in the galleries as described previously [36, 42, 46].

Firstly, various amount of Na^+-MMT clay was dispersed in 100 mL of deionized water using ultrasonication for 5 h to allow swelling of the Na^+-MMT clay. Then, 20 mL (0.21 mol) of aniline was added drop wise, followed by the addition of pre-cooled 1 M HCl. The mixture was stirred for 15–20 min until the aniline monomer was fully intercalated into the Na^+-MMT, and a clear dispersion was formed. Then, pre-cooled 11.5 g (0.05 mol) APS solution (dissolved in 1 M aqueous HCl) was added drop wise, and the mixture was stirred for another 4 h in an ice bath at 0 °C. The obtained dark blue green precipitate of the PANI/MMT composite was filtered out of the reaction mixture, and washed several times with deionized water and methanol to remove unreacted monomer and HCl and dried under vacuum at 80 °C for 24 h. For comparison, pure PANI in ES form was also synthesized under the same condition without adding MMT clay.

The PANI/MMT nanocomposites with various MMT content prepared within this study are referred in the following text as PNC-X, where X denotes the concentration in wt% of the clay with respect to the monomer amount in the reaction mixture (Table 1).

Characterizations

Wide-angle X-ray scattering (WAXS) pattern of pure MMT clay and PNC containing different concentrations of MMT clay were obtained using powder diffractometer HZG/4A (Freiberger Praezisionsmechanik GmbH, Freiberg) with Cu Kα radiation ($\lambda = 0.1542$ nm, 40 kV, 45 mA, Ni-filter, and reflection geometry). WAXS scans were performed at ambient temperature within the interval $1.4° < 2\theta < 20°$ with 0.1° step.

Field emission scanning electron microscopy (FESEM) images of pure PANI, MMT clay, and PNC were observed using a FESEM SUPRA 40VP, Carl Zeiss NTS GmbH, while high resolution transmission electron microcopy (HRTEM) images and selected area diffraction pattern (SADP) patterns were obtained with FEI Technai 20 U Twin transmission electron microscope at 200 kV. The following procedure for the sample preparation was adopted: PANI, MMT or PNC powders were first dispersed in THF using ultrasonication to get uniform dispersion that was subsequently drop cast on the carbon coated Cu grid and left to dry.

FTIR spectra were recorded on a Bruker spectrophotometer in the range 4,000–400 cm^{-1} with the resolution 2 cm^{-1}. Thermogravimetric analysis (TGA) was performed with Perkin Elmer TGA 7 thermogravimetric (TG) analyzer, operated with Pyris 1 Advanced Kinetics software. The measurements were performed from room temperature to 800 °C at a heating rate of 10 °C/min in the nitrogen atmosphere (N_2 flow 20 mL/min) or alternatively in air.

DC electrical conductivity was measured in ambient conditions at room temperature using two-probe method in a serial connection of the sample, electrometer Keithley 617, and home made stabilized DC power supply. The samples were in a form of pressed pellets prepared by press designed for IR samples preparation (diameter 1.3 cm, load 6.6 ton in air). The conductivity was calculated from the conductance taken in the linear part of volt–amp characteristics, the area, and distance between the electrodes.

Results and discussion

Synthesis and structure of prepared PANI/MMT nanocomposites

The intercalation and polymerization mechanism of PANI in the MMT environment is depicted in Fig. 1. The initial intercalation of the aniline monomer into the interlayer

Table 1 Polymerization characteristics and various parameters of prepared PANI/MMT nanocomposites

Sample	Clay loading (wt%) with respect to monomer amount (20 g)	PANI content in PNC[a] (wt%)	Peak angle 2 θ	Scattering vector q ($Å^{-1}$)	Interlayer d-spacing (nm)	Room temp. Conductivity σ_{rt} (S cm^{-1})
PANI–ES	0	100	–	–	–	1.6×10^{-4}
PNC-2.5	2.5	90	6.871	0.488	1.29	2.0×10^{-4}
PNC-5	5	81	5.991	0.425	1.48	2.4×10^{-4}
PNC-15	15	60	6.228	0.446	1.41	2.9×10^{-4}
PNC-25	25	44	6.663	0.473	1.33	7.4×10^{-4}
MMT	–	0	7.677	0.545	1.15	1.1×10^{-6}

[a] Determined by weight measurement

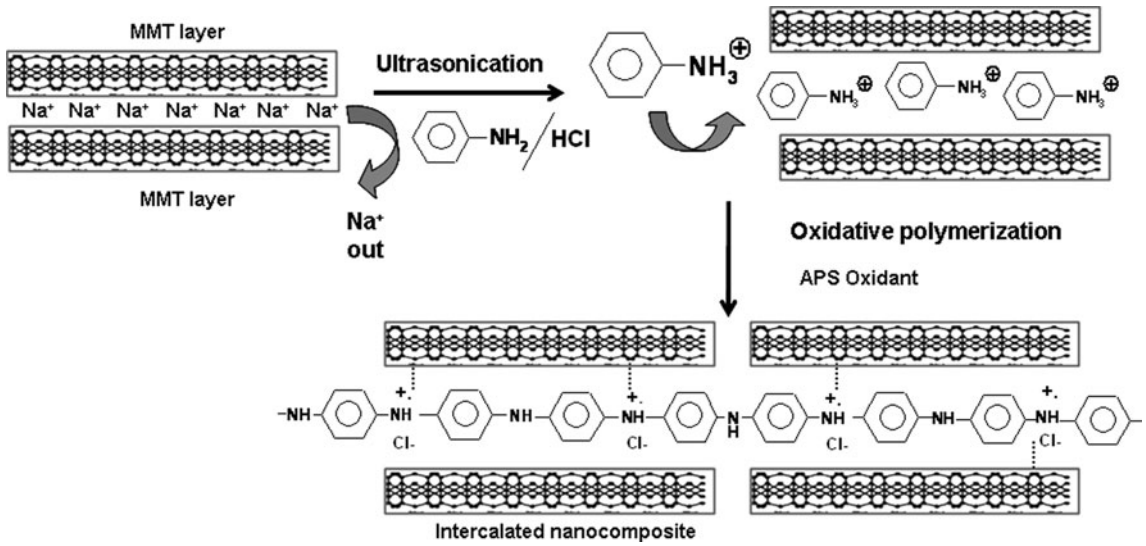

Fig. 1 Schematic route of the synthesis of intercalated PANI/MMT clay nanocomposites

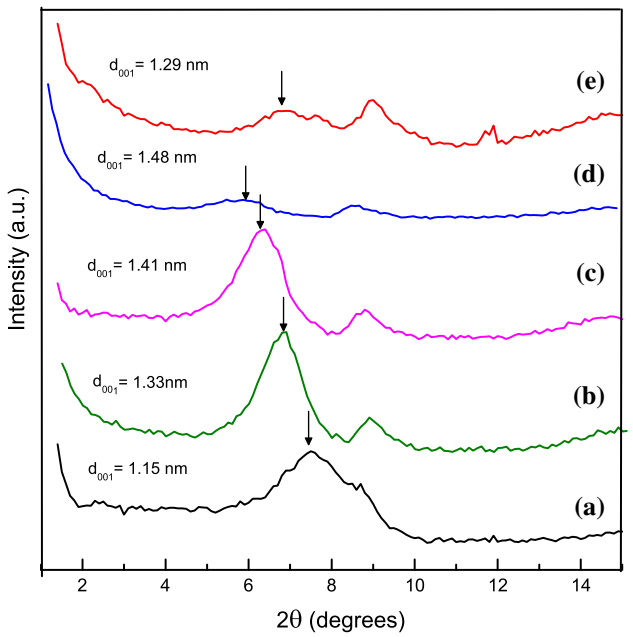

Fig. 2 WAXS pattern of **a** pure MMT clay, **b** PNC-25, **c** PNC-15, **d** PNC-5, and **e** PNC-2.5

spacing of the clay was driven by the exchange of Na^+ cations in the Na^+-MMT clay with anilinium cations. Their subsequent oxidative polymerization with APS yielded PANI in a form of emeraldine salt (ES). The degree of intercalation in synthesized intercalated nanocomposites was confirmed by the WAXS diffraction pattern (Fig. 2). The peak at $2\theta \approx 7.7^{o}$ observed for pure MMT (Fig. 2a) corresponds to the periodicity in the direction perpendicular to the (001) plane of the clay. In the PNCs (Fig. 2b–e), this peak was observed at lower 2θ values, indicating increased interplanar distance in the MMT crystals. The d-spacing values (d_{001}) were calculated from the peak position of WAXS pattern using Bragg's equation $d = 2\pi/q$, where q is the magnitude of scattering vector defined as $q = (4\pi/\lambda)\ \sin\ (\theta)$. λ is the X-ray wavelength, and 2θ is the scattering angle [46]. The position of (001) peak, and corresponding d-spacing are shown in Table 1. With the increase in PANI content (Fig. 2b–d), the d-spacing was first increased from the value $d_{001} = 1.15$ nm for pure Na^+-MMT clay up to the maximum value $d_{001} = 1.48$ nm, which reached for PNC-5 having about 81 wt% of PANI (Fig. 2d). At this concentration, the WAXS diffraction pattern is less resolved suggesting lower ordering of structure in the PNC. With further increase in PANI content, slight decrease of the interplanar spacing was observed to the value $d_{001} = 1.29$ nm for the PNC-2.5 (Fig. 2e). The diffraction patterns also exhibit a small peak corresponding to the undisturbed MMT, while no evidence for the exfoliation was found.

Previously published results on the changes of interplanar spacing of MMT with the PANI content are not consistent. For example, Lee et al. [46] reported the increase in basal spacing of MMT in the nanocomposites from 0.97 to 1.40 nm up to 12.5 wt% of PANI followed by a decrease at higher PANI content, while the same authors reported [42] the increase in basal spacing from 0.97 nm up to the 1.45 nm for 75% PANI content can be found. Further, Celik et al. [43] also reported the increase in basal spacing up to 1.52 nm at 75% PANI content, which is quite comparable to our results (Table 1).The maximum 0.4 nm expansion in the d_{001} spacing found in our study fits well to the values published on similar systems [35, 36, 42, 45, 46] and confirms the insertion of PANI chains between the silicate layers and the formation of intercalated

PANI/MMT nanocomposites as well as the limitation, and even decrease of the inter-plane spacing at higher PANI concentrations.

Morphology

Microstructures of the PANI/MMT composites, pristine MMT, and pure PANI as observed by FESEM are compared in Fig. 3a–d. The layered structure of pristine MMT is clearly observed (Fig. 3a), while pure PANI has a granular structure (clusters or globules) as seen in Fig. 3d. In the PNCs with increasing PANI content (Fig. 3b–c), the structure changes from prevailing plate-like structure to a globular one, pointing that at higher monomer/MMT ratio the polymerization is not limited only into the MMT galleries. PANI partially covers the clay platelets surface because of columbic interaction between the positive charge located at the nitrogen atom of PANI and negative charged on the surface of the clay. Moreover, at the excess of the monomer some part of it stays free in the reaction mixture and the polymerization can proceed partially in the bulk, yielding free polymer not anchored on the clay surface. The PANI-coated clay particles can be easily aggregated because of their large aspect ratio.

In order to identify the intercalated structures of the nanocomposites more clearly, we acquired high resolution transmission electron microscope (HRTEM) images for PNC-2.5 sample, as shown in Fig. 4 for different scale bars. Dark stripes represent the clay platelets (marked with arrows), and the gray/white areas represent the polymer matrix. Even at the lowest MMT content, the TEM image shows that the composite contains a considerable part of stacked layers, which is consistent with the results of X-ray diffractogram (Fig. 2e). SADP (inset of Fig. 4b) shows some diffusion rings, suggesting that the prepared composite contains non negligible fraction of the crystalline phase.

FTIR spectra

FTIR spectroscopy was used to investigate the chemical structure of the PNC and interactions between the PANI and MMT. Figure 5 shows the FTIR spectra of pure MMT clay, pure PANI (ES), and PNC samples with various clay loadings. The characteristic bands of pure MMT clay can be assigned according to the literature as 3629 cm^{-1} (ν_{O-H}), 3443 cm^{-1} (ν_{Mg-O}), 915 cm^{-1} (δ_{Al-OH}), 523 cm^{-1} ($\nu_{Si-O-Al}$), and 479 cm^{-1} ($\delta_{Si-O-Si}$) (Fig. 5d). The broad absorption band in the 1,350–750 cm^{-1} region involves four Si–O stretching modes of the MMT: three of them in plane (1,120; 1,048; and 1,025 cm^{-1}), and one out-of-plane mode (1,080 cm^{-1}) [47]. Pure PANI–ES (Fig. 5a) is characterized by the vibrations at 1,294 cm^{-1} (ν_{C-N} in secondary aromatic amine), 1,555 cm^{-1} ($\nu_{C=C}$, quinoid ring), 1,469 cm^{-1} ($\nu_{C=C}$, benzenoid ring), and 1,120 cm^{-1} (vibrational mode of B–NH^{+}=Q structure, which is formed

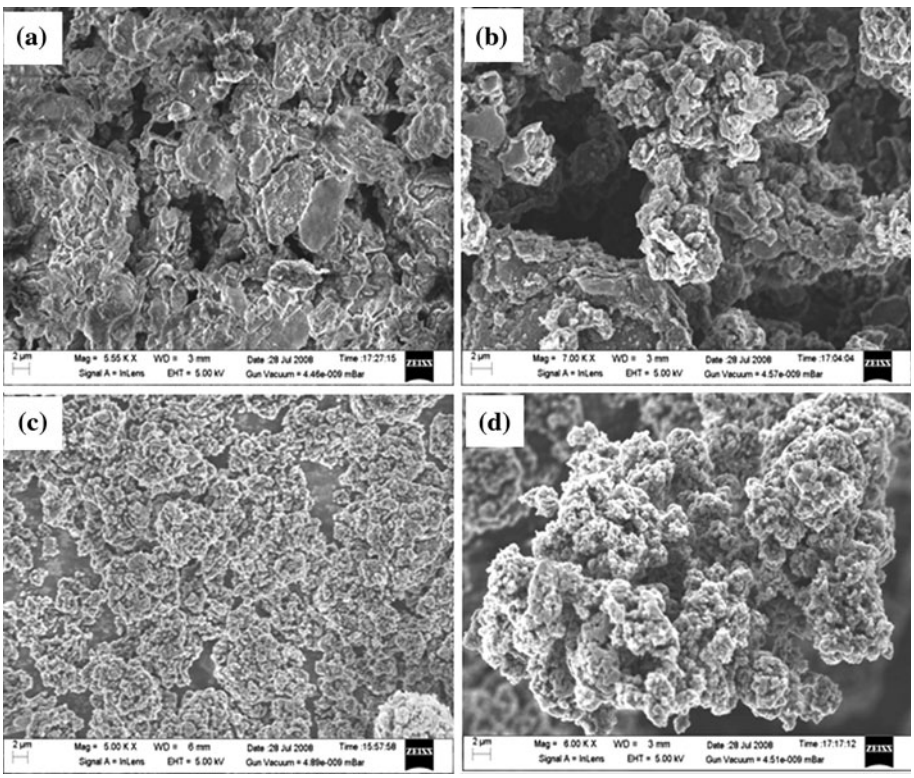

Fig. 3 FESEM images of **a** pure MMT, **b** PNC-25, **c** PNC-2.5, and **d** PANI–ES

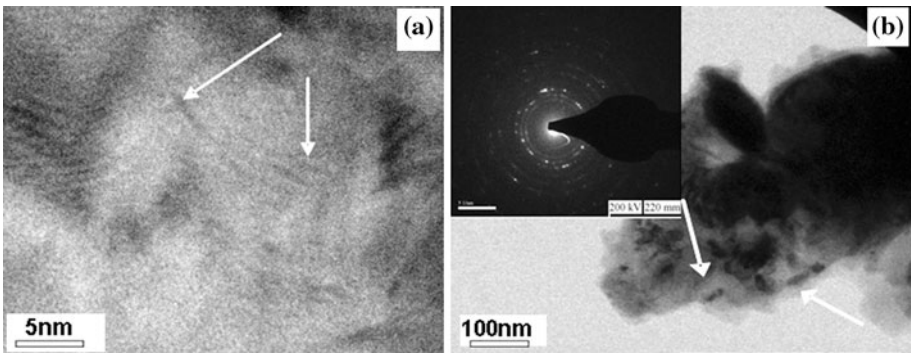

Fig. 4 HRTEM images and SADP pattern of PNC-2.5 shown at different *scale bars*. *White arrows* show the clay platelets

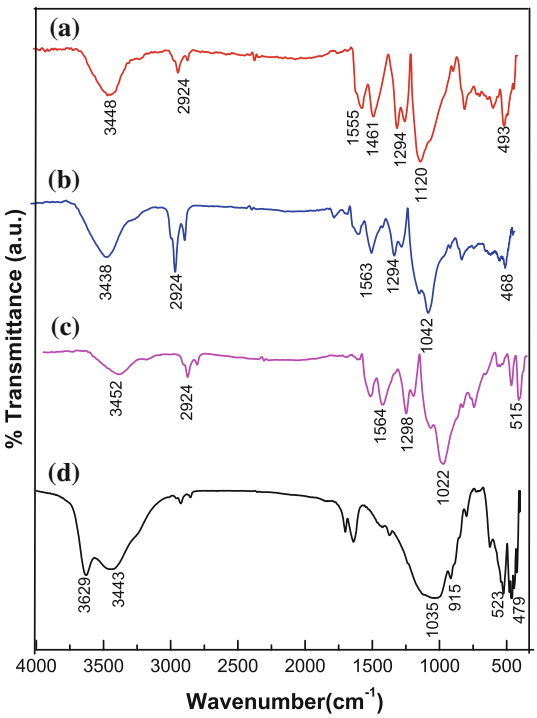

Fig. 5 FTIR Spectra of **a** pure PANI–ES, **b** PNC-2.5, **c** PNC-25, and **d** pure MMT clay

during protonation process and which is associated with an extended electron delocalization and increased electrical conductivity of PANI [42, 46, 48]. The spectrum of the PNC-2.5 composite (Fig. 5b) is dominated by the IR spectrum of the pure PANI–ES spectrum since the composite contains only minor fraction of the MMT. The increase of the relative peak intensity at 1042, 522, and 468 cm^{-1} can be explained as an overlap of the absorption bands of PANI with the strong absorption peaks of MMT. In the spectrum of PNC-25 composite (Fig. 5c), both the characteristic peaks of the clay and PANI are clearly visible, however, the spectral features in the regions 1,350–750 cm^{-1} cannot be explained using a simple superposition of both components. Cole [47] used FTIR spectroscopy for characterizing the state of the intercalation and exfoliation in polymer nanocomposites prepared from montmorillonite-based nanoclays. The authors stated that the Si–O-stretching band envelope is affected by both the chemistry of the montmorillonite and the presence of intercalant. It was shown that the shape of the clay band envelope in the 1,350–750 cm^{-1} region changes with the degree of processing because of the changes in the quality of intercalation/exfoliation. He showed that out-of-plane Si–O mode of MMT near 1,070–1,080 cm^{-1} is particularly sensitive and can be considered as an indicator of the clay intercalation in a polymeric matrix. In another study [49], the Si–O bands envelope was analyzed in detail by decomposing it into four components: peak I (1,115 cm^{-1}), II (out-of-plane mode, 1080 cm^{-1}), III (1,045 cm^{-1}), and IV (1,024 cm^{-1}), and it was found that the shape and position of these peaks changes with the variation of water content, the greatest shift being observed for the peak II that becomes more prominent as the interlayer spacing increases because of their separation by adsorbed water. In generally, in unintercalated MMT clay the band associated with the out-of-plane Si–O vibration is broadened due to coupling of vibrations from the closely packed adjacent layers. As these layers become separated from each other, this coupling effect is suppressed and the narrowing of the absorption band occurs. In addition, it can be expected that the in-plane Si–O vibration mode in the silica in the tetrahedral layer could be restricted because of the interaction with intercalant. As a result, the corresponding absorption bands can be narrowed [47, 49]. This maybe the case of the MMT intercalated with PANI, where the formation of hydrogen bonding between the basal oxygen and nitrogen atom in PANI polymer can be expected. The analysis of the IR spectra of these nanocomposites is complicated because of the fact that in the region in which both the polymer and MMT are most sensitive to the structural and chemical changes like protonation, hydrogen bonding or intercalation, the characteristic bands of MMT and PANI overlap. Nevertheless, the narrowing of Si–O band envelope between 1,100 and 1,000 cm^{-1} in PNC may be used as an

evidence for the efficient intercalation of PANI between the clay layers.

Thermogravimetric analysis (TGA)

The incorporation of clay into the polymer matrix is known for enhancing the thermal stability of the nanocomposite by acting as a barrier against the penetration of oxygen into the specimen and diffusion of the volatile products generated during decomposition out of the composite. Figures 6 and 7 show the TG curves and their corresponding derivatives, DTG, (inset of Figs. 6, 7) for the pure PANI–ES and for PNC samples containing various amount of clay, measured in air and nitrogen atmosphere, respectively. Pure PANI shows three temperature regions of the weight loss process as seen from the TG and corresponding three minima in DTG curves (Figs. 6, 7 inset), indicating the weight loss at each step. The first weight loss region found below 100 °C is attributed to the loss of water and alcohol moieties, and the second one observed in the interval 200–300 °C is explained by the elimination of acid dopant (HCl) [24–27]. The third and major weight loss process (80% of the total weight loss) starts at around 350 °C (in air) and at 400 °C (in nitrogen atmosphere), and it has been assigned to the thermal decomposition of PANI backbone [24–27, 42, 43]. In order to distinguish the PANI stability in the composites from the weight losses of other origins, a careful analysis of the third peak of the DTG spectra was performed, namely the degradation of PANI was calculated as an integral of the corresponding peak. The values for the T_{DTG} (the temperature at the minimum

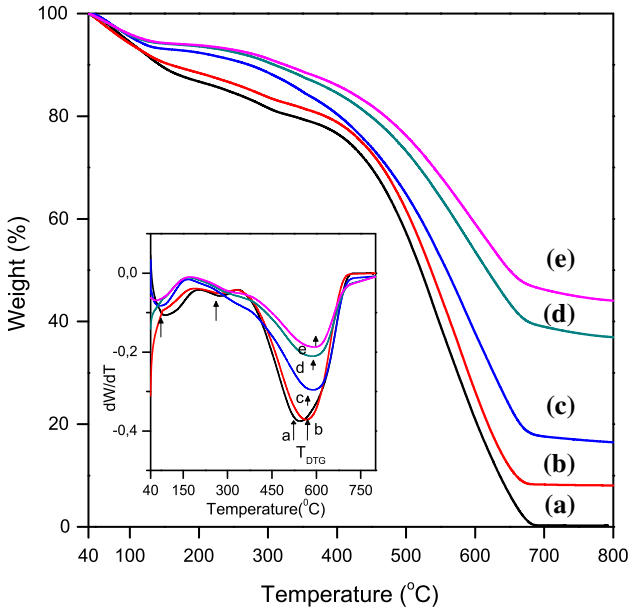

Fig. 6 TGA and DTG curves (inset) of **a** pure PANI–ES, **b** PNC-2.5, **c** PNC-5, **d** PNC-15, and **e** PNC-25 in air at heating rate 10 °C/min

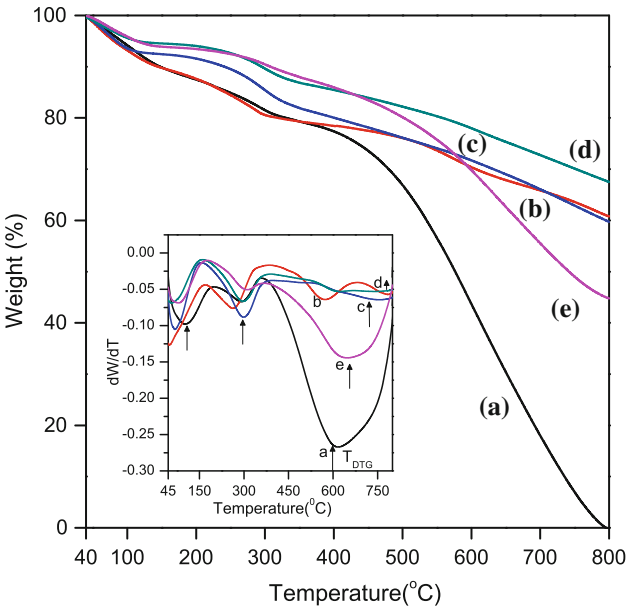

Fig. 7 TGA and DTG curves (inset) of **a** pure PANI–ES, **b** PNC-2.5, **c** PNC-5, **d** PNC-15, and **e** PNC-25 in nitrogen (N_2) atmosphere at heating rate 10 °C/min

of DTG curves corresponding to third weight loss temperature region) and the weight loss due to PANI in PNCs are summarized in Table 2. It can be seen that in oxidative degradation (Fig. 6), as the concentration of MMT clay is increased, the total weight loss of the PNC systematically decreases with decreasing PANI fraction in the nanocomposite. On the other hand, in non-oxidative degradation (Fig. 7), the weight loss is not decreased systematically. The inset (Figs. 6, 7) and Table 2 show the temperature at the minimum of DTG curve (T_{DTG}) for pure PANI–ES in air atmosphere is ≈540 °C (600 °C under N_2), attributable to the thermal scission of PANI backbone chains, which shifts to higher temperature in all PNC samples with respect to the clay concentration. The shifting of T_{DTG} in PNCs confirms that intercalated nanocomposites are more thermally stable than the pure PANI system.

For lower to medium clay fractions, it is noticeable that the amplitude of total weight loss is lower in N_2 than in air atmosphere. The increased stability of the composites in N_2 atmosphere for medium clay concentrations may derive from the barrier effect caused by limited escape of the volatile thermo-oxidation products outside the sample as well as by the limited oxygen diffusion inside the PNC.

In case of PNC-25, containing higher clay amount, the total weight loss in air and in N_2 is similar. The decreased stabilization effect of the MMT in PNCs with higher MMT content maybe explained by the inhomogeneity of the PNC, in which some of the PANI chains reside outside the silicate layers of MMT and facilitate the diffusion of oxygen or products of thermal

Table 2 TG and DTG results of pure PANI–ES and PNC with different clay loading in air and N_2

Sample	PANI content in PNC-MMT (wt%)	Third major weight loss (%) (in air)	Third major weight loss (%) (in N_2)	T_{DTG} (°C) (in air)	T_{DTG} (°C) (in N_2)
PANI–ES	100	80	80	540	600
PNC-2.5	90	73	17	565	570
PNC-5	81	66	21	589	615
PNC-15	60	49	18	585	622
PNC-25	44	43	42	594	650

T_{DTG} is the temperature at the minimum of DTG curve with regard to the third weight loss

decomposition inside/outside the specimen. It can be easily rationalized by the incomplete disintegration of the MMT powder in the reaction mixture by sonication before the aniline polymerization. As a result, polymerization proceeds with higher probability in the bulk outside the MMT galleries. It is in accordance with the observations made by XRD and SEM.

The enhanced oxidative and non-oxidative thermal stability of the PANI nanocomposites can be attributed to the restricted thermal motion of the PANI in the gallery of the MMT clay (i.e., improved barrier property). These results are in good agreement with the results for PANI/MMT nanocomposites [24–27, 42, 43], and proves that the intercalated nanostructure in PANI and layered silicate nanocomposites is crucial to the enhanced thermal stability in air as well as in the inert atmosphere.

Electrical conductivity

The dependence of the electrical conductivity (σ_{rt}) on the PANI content measured at room temperature is shown in Fig. 8 and the values for pure PANI, MMT, and PNCs with various PANI content are summarized in Table 1. The conductivity of pure MMT, $\sigma_{rt} = 10^{-6}$ S cm^{-1}, fits well within the conductivity limits published in the literature [44], and it is of a ionic origin. The conductivity of pure PANI prepared at the same conditions as the polymerization of aniline in the PNCs was measured as 1.6×10^{-4} S cm^{-1}. Surprisingly, the conductivity of PNCs was found higher than that of pure PANI, reaching the maximum value, 7.4×10^{-4} S cm^{-1}, for the concentration 44 wt. % of the PANI content in the nanocomposite. The results on the conductivity of similar composites published in the literature are rather scattered. Even higher values $\sigma_{rt} = 10^{-3}$ S cm^{-1} were reported in the literature for the PANI/MMT composite containing 7.2 wt% PANI [36] or $\sigma_{rt} = 10^{-1}$ Scm^{-1} for the nanocomposite containing 80 wt% PANI [31]. In the latter case, the conductivity of pure PANI was about 10^{-4} S cm^{-1}. Lee et al. reported $\sigma_{rt} = 10^{-1}$ S cm^{-1} for the composite with 74.7 wt% of PANI, but in this case the composites had a lower conductivity than the pristine PANI with $\sigma_{rt} = 1.5$ S cm^{-1} [42]. However, the values reported by various authors are difficult to compare since they are influenced by the PANI polymerization method, reaction media, and the oxidant used.

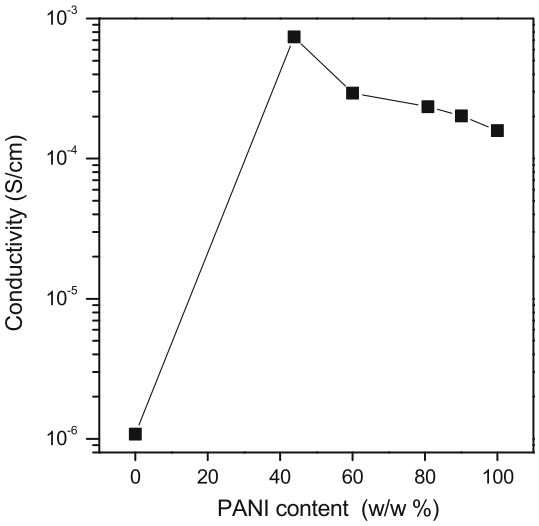

Fig. 8 Room temperature conductivity (σ_{RT}) of PANI/MMT nanocomposites as a function of PANI content

The conductivity of the PNC is composed of the ionic conductivity of MMT originated in Na^+ cations that was inherently contained in MMT and by residual traces of water, and of the electronic conductivity of the oxidized form of PANI. In the pure MMT, the surplus charge on the surface of clay layers is compensated by interlayer Na^+ cations. When aniline monomer is added into the reaction mixture, the anilinium molecules are intercalated into the clay galleries and replaced the Na^+ cations. At higher amount of clay in the reaction mixture, these cations are not replaced completely, hence they contribute to the overall ionic conductivity.

However, the ionic conductivity is of several orders of magnitude smaller than the observed conductivity of the nanocomposites, and its contribution should not cause detectable increase of the conductivity compared with pure PANI. Alternative explanation could be found in the morphology changes of the PANI in the presence of MMT. It has been shown previously that conductive polymers show an enhancement of the conductivity when confined

between clay lamellas, as at this condition the distortion of polymer chains is prevented [23, 41, 50]. Better ordering of the conductive polymer can give rise to higher conductivity.

Conclusion

X-ray diffractograms together with electron microscopy techniques and FTIR spectra confirm the efficient intercalation of electrically conductive PANI between inorganic clay layers during the in situ intercalative oxidative polymerization of aniline with Na^+-MMT. No exfoliation was observed even at a low clay concentration, but only wider distribution of inter planar distances occurred at PANI concentrations above 80% with the presence of a fraction of MMT with shorter interplanar distances than in medium PANI concentration. The employed route offers the possibility to improve the thermal properties with simultaneously controlled electrical conductivity. Depending on the loading of the clay, the room temperature conductivity values of these nanocomposites varied between 2.0×10^{-4} and 7.4×10^{-4} S cm^{-1}. Contrary to some previously published results, the conductivity showed the highest values at medium PANI concentration and decreased with increasing PANI content. The decrease in conductivity at high PANI concentration was ascribed to the decrease of the structure ordering of PANI in the nanocomposites. The improved thermal stability along with the increased conductivity of these nanocomposites and enhanced mechanical properties maybe of immense interest in many applications like EMI shielding material or polymer electrodes for batteries and solar cells.

References

1. MacDiarmid AG, Epstein AJ (1994) Synth Met 65:103
2. Stejskal J, Hlavatá D, Holler P, Trchová M, Prokeš J, Sapurina I (2004) Polym Int 53:294
3. Guo T, Wang LS, Evans DG, Yang WS (2010) J Phys Chem C 114:4765
4. Chen YP, Yang G, Zhang ZH, Yang XY, Hou WH, Zhu JJ (2010) Nanoscale 2:2131
5. Njuguna J, Pielichoski K (2004) J Mater Sci 39:4081. doi:10.1023/B:JMSC.0000033387.51728.de
6. Reena VL, Pavithran C, Verma V, Sudha JD (2010) J Phys Chem B 114:2578
7. Cai JJ, Zuo PJ, Cheng XQ, Xu YH, Yin GP (2010) Electrochem Commun 12:1572
8. Li QH, Wu JH, Tang QW, Lan Z, Li PJ, Lin JM, Fan LQ (2008) Electrochem Commun 10:1299
9. Shi S, Zhang L, Li J (2009) J Mater Sci 44:945. doi:10.1007/s10853-008-3207-8
10. Chang K-C, Lai MC, Peng CW, Chen YT, Yeh JM, Lin CL, Yang JC (2006) Electrochim Acta 51:5645
11. Wang J, Chan S, Carlson RR, Luo Y, Ge GL, Ries RS, Heath JR, Tseng HR (2004) Nano Lett 4:1693
12. Deepa M, Ahmad S, Alam J, Ahmad S, Sood KN, Srivastava AK (2007) Electrochim Acta 52:7453
13. Scully SF, Bissessur R, Dahn DC, Xie GH (2010) Solid State Ionics 181:933
14. Li ZF, Ruckenstein E (2002) Langmuir 18:6956
15. Kerr TA, Wu H, Nazar LF (1996) Chem Mater 8:2005
16. Manrıquez V, Galdamez A, Ponce J, Brito I, Kasaneva J (1999) Mater Res Bull 34:123
17. Zang D, Qin J, Yakushi K, Nakazawa Y, Chimura KI (2000) Mater Sci Eng A 286:183
18. Bissessur R, White W, Dahn DC (2006) Mater Lett 60:248
19. Liu Y, Chen ZM, Xie TX, Yang GS (2011) J Mater Sci 46:2700. doi:10.1007/s10853-010-5138-4
20. Sudhakara P, Kannan P, Obireddy K, Rajulu AV (2011) J Mater Sci 46:2778. doi:10.1007/s10853-010-5152-6
21. Chen-Yang YW, Yang HC, Li GJ, Li YK (2004) J Polym Res 11:275
22. Maji PK, Guchhait PK, Bhowmick AK (2009) J Mater Sci 44:5861. doi:10.1007/s10853-009-3827-7
23. Mehrotra V, Giannelis EP (1991) Solid State Commun 77:155
24. Pielichowski K (1997) Solid State Ionics 104:123
25. Narayanan BN, Koodathil R, Gangadharan T, Yaakob Z, Saidu FK, Chandralayam S (2010) Mater Sci Eng B 168:242
26. Marjanovic GC, Dondur V, Milojevic M, Mojovic M, Mentus S, Radulovic A, Vukovic Z, Stejskal J (2009) Langmuir 25:3122
27. Lee D, Char K (2002) Polym Degrad Stab 75:555
28. Kim B-H, Jung J-H, Hong S-H, Joo J, Epstein AJ, Mizoguchi K, Kim JW, Choi HJ (2002) Macromolecules 35:1419
29. Kim BH, Jung JH, Hong SH, Kim JW, Choi HJ, Joo J (2001) Curr Appl Phys 1:112
30. Song DH, Lee HM, Lee KH, Choi HJ (2008) J Phys Chem Solid 69:1383
31. Lee HM, Choi HJ (2007) Mol Cryst Liq Cryst 463:503
32. Chang K-C, Jang G-W, Peng C-W, Lin C-Y, Shieh J-C, Yeh J-M, Yang J-C, Li W-T (2007) Electrochim Acta 52:5191
33. Do Nascimento GM, Padilha ACM, Constantino VRL, Temperini MLA (2008) Colloids Surf A Physicochem Eng Aspects 318:245
34. Sun F, Pan YH, Wang J, Wang Z, Hu CP, Dong QZ (2010) Polym Compos 31:163
35. Do Nascimento GM, Constantino VRL, Temperini MLA (2002) Macromolecules 35:7535
36. Wu Q, Xue Z, Qi Z, Wang F (2000) Polymer 41:2029
37. Yoshimoto S, Ohashi F, Ohnishi Y, Nonami T (2004) Synth Met 145:265
38. Abbes IB, Srasra E (2010) React Funct Polym 70:11
39. Chen KH, Yang SM (2003) Synth Met 135–136:151–152
40. Yang SM, Chen KH (2003) Synth Met 135–136:51–52
41. Jia W, Segal E, Kornemandel D, Lamhot Y, Narkis M, Siegmann A (2002) Synth Met 128:115
42. Lee D, Char K, Lee SW, Park YW (2003) J Mater Chem 13:2942
43. Celik M, Onal M (2007) J Polym Res 14:313
44. Do Nascimento GM, Constantino VRL, Landers R, Temperini MLA (2006) Polymer 47:6131
45. Bober P, Stejskal J, Špírková M, Trchová M, Varga M, Prokeš J (2010) Synth Met 160:2596
46. Lee D, Lee S-H, Char K, Kim J (2000) Macromol Rapid Commun 21:1136
47. Cole KC (2008) Macromolecules 41:834
48. Kazim S, Ali V, Zulfequar M, Haq MM, Husain M (2007) Curr Appl Phys 7:68
49. Yan L, Roth CB, Low PF (1996) Langmuir 12:4421
50. Liu BYC, Tsai CJ (2003) Chem Mater 15:320